# Deep-learning based motion-corrected image reconstruction in 4D magnetic resonance imaging of the body trunk

Thomas Küstner[1,2], Jiazhen Pan[3], Christopher Gilliam[4], Haikun Qi[2], Gastao Cruz[2], Kerstin Hammernik[5], Bin Yang[3], Thierry Blu[6], Daniel Rueckert[5], René Botnar[2], Claudia Prieto[2], Sergios Gatidis[1]

[1]Medical Image And Data Analysis (MIDAS), Department of Diagnostic and Interventional Radiology, Tübingen, Germany.
[2]School of Biomedical Engineering and Imaging Sciences, King's College London, St. Thomas' Hospital, London, UK.
[3]Institute of Signal Processing and System Theory, University of Stuttgart, Stuttgart, Germany.
[4]RMIT University, Melbourne, Australia.
[5]Department of Computing, Imperial College London, London, United Kingdom.
[6]Chinese University Hong Kong, Hong Kong, Hong Kong.

***Abstract* — Respiratory and cardiac motion can cause artifacts in magnetic resonance imaging of the body trunk if patients cannot hold their breath or triggered acquisitions are not practical. Retrospective correction strategies usually cope with motion by fast imaging sequences with integrated motion tracking under free-movement conditions. These acquisitions perform sub-Nyquist sampling and retrospectively bin the data into the respective motion states, yielding subsampled and motion-resolved k-space data. The motion-resolved k-spaces are linked to each other by non-rigid deformation fields. The accurate estimation of such motion is thus an important task in the successful correction of respiratory and cardiac motion. Usually this problem is formulated in image space via diffusion, parametric-spline or optical flow methods. Image-based registration can be however impaired by aliasing artifacts or by estimation from low-resolution images. Subsequently, any motion-corrected reconstruction can be biased by errors in the deformation fields. In this work, we propose a novel deep-learning based motion-corrected 4D (3D spatial + time) image reconstruction which combines a non-rigid registration network and a (3+1)D reconstruction network. Non-rigid motion is estimated directly in k-space based on an optical flow idea and incorporated into the reconstruction network. The proposed method is evaluated on in-vivo 4D motion-resolved magnetic resonance images of patients with suspected liver or lung metastases and healthy subjects.**

## I. Introduction

In clinical diagnostics, magnetic resonance imaging (MRI) is a valuable and versatile tool. Its capability of assessing anatomy and functional processes within the human body in a non-invasive manner makes it an essential imaging modality. However, MRI is prone to a number of artifacts which can deteriorate image quality significantly. Due to its long acquisition time, motion is one of the major extrinsic factors influencing image quality. Motion patterns can be categorized into rigid motion (global translations or rotations of stiff structures) which arises from movements of whole body parts and non-rigid motion (local deformations of tissues) which mainly occurs in the thorax and abdominal region caused by physiological motion. Nevertheless, other body parts can be affected as well. Patient and physiological motion induces aliasing along the phase-encoding direction and/or blurring of the image content (depending on the imaging trajectory).

Motion visualization, estimation and correction are thus important tasks when processing MRI data. Fast and accurate motion estimation is required to enable prospective or retrospective motion correction techniques which can be applied to for example image guided interventions [1], cardiac assessment [2] or magnetic resonance (MR)-based motion correction of PET data [3, 4]. Several prospective and retrospective motion correction methods have been developed which include fast imaging sequences [5, 6], tracking of motion by sensors (MR navigators [7-12], cameras [13], respiratory belts or electrocardiogram [14]), application of motion-robust acquisition schemes [15], prospectively corrected acquisitions [16] and motion-resolved imaging [17-20].

One can thereby differentiate between the correction of rigid motion (e.g. head motion) and non-rigid periodic motion such (e.g. respiratory motion). Rigid motions can be tracked by MRI or other external sensors, directly modelled in k-space as linear phase drifts and incorporated into the acquisition (prospective correction) or reconstruction (retrospective correction) schemes. Non-rigid motion on the other hand is more challenging as it involves local deformations in image space which are related to changes in k-space (acquisition space) in a non-trivial way. Correction of non-rigid motion usually involves two steps: image reconstruction and image registration which will be explained in the following.

Data acquisition for these applications are usually accelerated by Parallel Imaging or Compressed Sensing yielding sub-Nyquist sampled (in the following denoted as subsampled) k-space data. In order to reconstruct aliasing-free images these methods rely on reconstruction schemes that for example incorporate sparsity or low-rank constraints to solve the ill-

posed problem [6, 21]. Fixed sparsity assumptions in Compressed Sensing are often too restrictive and incapable of fully modelling spatio-temporal dynamics. Careful fine-tuning between regularization and data consistency is required and especially in highly subsampled cases residual aliasing may remain in the image or over-regularization can occur leading to staircasing or blurring artifacts which affect the image registration.

After reconstruction, non-rigid motion fields can be estimated in image space from reconstructed images by solving a registration problem. A particular interest and challenge lies in the derivation of reliable 3D motion fields which capture the spatio-temporal non-rigid deformations, such as respiratory or cardiac movement. The non-rigid motion estimation problem can be formulated in image space using diffusion-based [22], parametric spline-based [23] or optical flow-based methods [24].

Instead of performing these two steps sequentially, motion-compensated image reconstruction schemes [25-31] integrate both motion field estimation and motion correction into the reconstruction process. These methods require reliable motion-resolved images from which the motion fields can be estimated. Motion field estimation can be controlled or supported by external motion surrogate signals [25, 26], initial motion field estimates [27, 28], from motion-aliased images [30] or low-frequency image contents [31]. Moreover, spatio-temporal redundancies can be exploited to achieve an aliasing-free image [32-38]. While these methods have been proven to be more robust against registration errors, they can require a significantly increased computational demand and/or achievable imaging acceleration is limited.

In case of highly subsampled data, aliasing artifacts in the reconstructed images can impair the registration process as reconstruction errors can propagate into the image registration and/or low-resolution images do not provide sufficient information for accurate registration. Moreover, higher subsampling leads to a challenging ill-posed reconstruction for which inherent spatio-temporal redundancies need to be better exploited. It would be desirable to carry out an aliasing-free registration in k-space directly from accelerated acquisitions to avoid any of these problems.

Recently deep-learning based reconstruction methods have gained attention to solve non-linear and underdetermined optimizations efficiently [39-42]. Proposed methods range from derivations of classical optimizations (e.g. ADMM-Net) [43], over cascaded convolutional networks [44-46], UNet-based convolutional networks [47] and recurrent neural networks [48] to generative adversarial network-based denoising (e.g. DAGAN) [49, 50], manifold learning [51], variational neural networks [52-54] and generalized PI reconstructions [55-57]. Network inputs thereby differ from single-coil 2D image [44-46] and/or k-space [43, 44, 51] to multi-coil 2D image [50, 53, 58, 59], 2D k-space [46, 47, 55-57, 60] or low-resolution 3D k-space [61] and were studied for static imaging [41, 43, 44, 46, 47, 49-54, 58], i.e. no temporal dynamics, or for 2D dynamic imaging [45, 48, 59], i.e. 2D + time such as 2D cardiac CINE, with complex-valued data handled as separate channels [45, 47, 52, 54, 59] or networks [58]. Recently, works investigated the possibility to combine reconstruction networks with image-based registrations [62, 63].

In this work, we propose a novel motion-corrected 4D (3D spatial + time) reconstruction network that exploits spatio-temporal redundancies by a sequence of 3D spatial and 1D temporal convolutions, in the following denoted as (3+1)D. Additionally, motion deformations are considered in the reconstruction which are obtained from a non-rigid registration network to enhance data-consistent information sharing among motion states. Non-rigid registration is directly formulated in k-space based on optical flow equations and the obtained motion fields are incorporated into a motion-corrected image reconstruction network. We will first describe the basic concepts on the image-based 3D non-rigid registration, denoted as Local All-Pass (LAP) which we have presented previously [4, 64, 65]. We then illustrate its extension to k-space based 3D non-rigid registration [66]. We propose a deep-learning based (3+1)D motion-corrected reconstruction network that incorporates the estimated motion fields. The proposed method is compared against an image-based registration and motion-corrected iterative SENSE reconstruction [27]. We investigate the proposed approach in 36 patients with suspected liver or lung metastases and 20 healthy subjects for retrospectively subsampled data of 3D motion-resolved MR imaging.

## II. Material and Methods

The proposed deep-learning architecture is depicted in Fig. 1. The network consists of two sub-networks: A non-rigid registration network which provides the motion fields and a (3+1)D reconstruction network which includes the estimated motion in the data consistency block to reconstruct an aliasing-free and motion-corrected image. Subsampled and motion-resolved k-spaces $\nu \in \mathbb{C}^{N_x N_y N_z N_t N_{Ch}}$ serve as input from which 3D non-rigid deformation fields $\underline{u} \in \mathbb{R}^{N_x N_y N_z N_t \times 3}$ are estimated. $N_x$, $N_y$ and $N_z$ reflect the 3D spatial dimensions, $N_t$ the temporal direction and $N_{Ch}$ the channels of the multi-coil MR receiver. The coil sensitivity map $S \in \mathbb{C}^{N \times N}$ with $N = N_x N_y N_z N_{Ch}$ is derived from the k-space $\nu$. The SENSE combined subsampled 4D image $\rho_u \in \mathbb{C}^{N_x N_y N_z N_t}$ is reconstructed to an aliasing-free and motion-corrected image $\rho \in \mathbb{C}^{N_x N_y N_z N_t}$ for each motion state.

### A. *In-vivo 4D MR acquisition*

Motion-resolved k-space data was obtained on a cohort of 36 patients (60 ± 9 years, 20 female) with suspected liver or lung metastases and 20 healthy subjects (31 ± 4 years, 9 female) [4]. The study was approved by the local ethics committee and all subjects gave written consent.

A 3D T1 weighted spoiled gradient echo sequence was acquired in coronal orientation with a variable-density Poisson Disc subsampling [67] for an acquisition time of 90 seconds (prospectively subsampled) and 300 seconds (reference). The remaining imaging parameters were TE = 1.23ms, TR = 2.60ms, bandwidth = 890Hz/px and a flip angle of 7°. A matrix

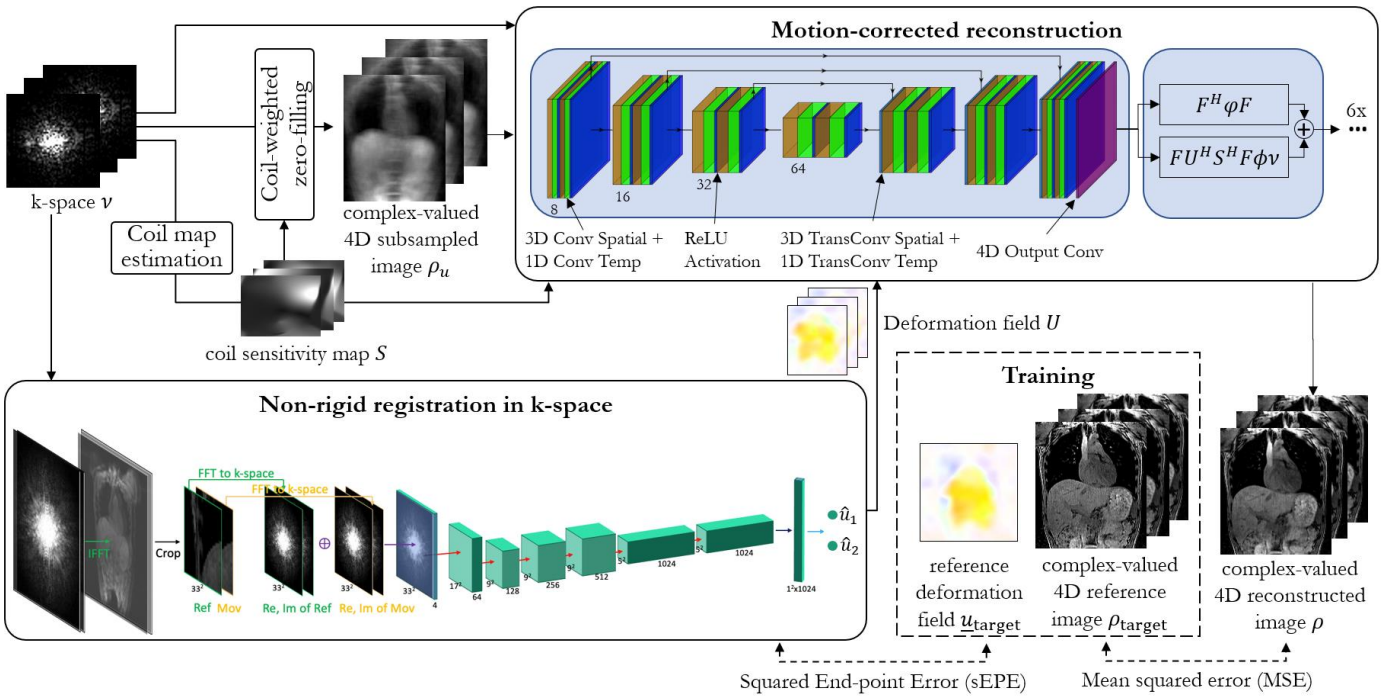


Fig.1: Proposed motion-compensated 4D reconstruction network which consists of two sub-networks: A non-rigid registration network directly operating on motion-resolved k-spaces and a reconstruction network employing 3D spatial and 1D temporal convolutions to exploit spatio-temporal redundancies. The estimated deformation fields are incorporated in the data consistency blocks. A coil-weighted zero-filled image $\rho_u$ is inputted together with the auto-calibrated coil sensitivity maps $S$, the k-space $\nu$ and the deformation fields $U$ to reconstruct a motion-corrected image $\rho$ for each motion state. During training, target images from a separate reference acquisition and target deformation fields derived via Local All-Pass are used to minimize the mean squared error (MSE) and end-point error (EPE), respectively.

size of $N_x \times N_y \times N_z = 256$ x 256 x 144 (RO x PE x 3D $\Leftrightarrow$ HF x LR x AP) was acquired covering a field-of-view of 500 x 500 x 360 mm$^3$. A 2D MR self-navigation signal (256 x 8 x 1, RO x PE x 3D) was acquired each 200 ms serving as gating signal. MR data were retrospectively gated into $N_t = 8$ respiratory gates, ranging from end-expiratory to end-inspiratory position, with a Gaussian view-sharing amongst neighbouring gates. An average acceleration factor per motion gate of ~14x (prospectively subsampled) and ~4x (reference) was obtained. The coil sensitivity map was obtained from the time-averaged fully sampled calibration center region by ESPIRIT [68] with virtual coil compression to a common size of $N_{Ch} = 8$.

Training data for the registration network was generated by an iterative SENSE reconstruction [69] of the reference data followed by LAP registration [64, 65] to retrieve the target deformation field $\underline{u}_{\text{target}}$. End-expiratory target images $\rho_{\text{target}}$ for the reconstruction network were obtained from a motion-corrected iterative SENSE reconstruction of the reference data [27]. Overall, 50 subjects (33 patients and 17 healthy subjects) were used for training and 6 subjects (3 patients and 3 healthy subjects) were used in testing. For training, the reference data was used while for testing the prospectively subsampled data was taken.

### *B. Non-rigid registration in k-space*

The key idea of LAP is that any non-rigid deformation can be regarded as local rigid displacements. These displacements can be modeled as local all-pass filter operations. Under the assumption of local brightness consistency, the optical flow equation of a rigid displacement can be equivalently stated in Fourier space

$$\rho_r(\underline{x}) = \rho_m(\underline{x} - \underline{u}) \iff \nu_r(\underline{k}) \simeq \nu_m(\underline{k}) e^{-j\underline{u}^T \underline{k}} \qquad (1)$$

for deforming a moving image $\rho_m$ to a reference image $\rho_r$ via a deformation field $\underline{u}(\underline{x})$ at position $\underline{x} = [x, y, z]^T$, with $\nu_r(\underline{k})$ and $\nu_m(\underline{k})$ being the k-spaces entries of the moving and reference image at location $\underline{k} = [k_x, k_y, k_z]^T$. The linear phase ramp can be regarded as an all-pass filter $\hat{h}(\underline{k}, \underline{x}) = e^{-j\underline{u}^T(\underline{x})\underline{k}} = \hat{p}(\underline{k})/\hat{p}(-\underline{k})$ that can be split into a forward $\hat{p}(\underline{k})$ and backward filter $\hat{p}(-\underline{k})$ with $p(\underline{x}) \in \mathbb{R}$ which is all-pass by design [70]. Global non-rigid deformation is then modelled as local rigid displacements and hence the problem of non-rigid image registration is transformed to estimating the appropriate local all-pass filter for different $\underline{x}$ in a cubic window $\mathcal{W}$. Selecting an optimal filter basis $p_n$ that fulfills diffeomorphic and smooth flow (e.g. Gaussian), allows to conclude the registration formulation in image domain

$$\min_{\{c_n\}} \sum_{\underline{x}\in\mathcal{W}} \mathcal{D}\left[\mathcal{W}(\underline{x})\cdot\left(p(\underline{x}) * \rho_m(\underline{x})\right), \mathcal{W}(\underline{x}) \cdot\left(p(-\underline{x}) * \rho_r(\underline{x})\right)\right] \quad \text{s.t. } p(\underline{x}) = p_0(\underline{x}) + \sum_{n=1}^{N} c_n p_n(\underline{x}) \quad \forall \underline{x} \in \mathbb{R}^3 \tag{2}$$

for which at each image position $\underline{x}$ the $N$ optimal filter coefficients $c_n$ are estimated [71] by minimizing the dissimilarity $\mathcal{D}$ (e.g. mean-squared-error, MSE) between $\rho_m$ and $\rho_r$.

In order to carry out the operations in the Fourier domain (i.e. k-space), we need to consider the local windowing $\mathcal{W}$

$$\rho_W(\underline{x}) = \mathcal{W}(\underline{x})\cdot\rho(\underline{x}) \Leftrightarrow \nu_W(\underline{k}) = T(\underline{k}) * \nu(\underline{k}) \tag{3}$$

which corresponds in k-space to the convolution by a phase-modulated (for various $\underline{x}$ positions) tapering function $T(\underline{k})$. Transforming (2) in Fourier domain

$$\min_{\{c_n\}} \sum_{\underline{k}\in\mathbb{R}^3} \mathcal{D}\left(T(\underline{k}) * \left(\hat{p}(\underline{k})\nu(\underline{k})\right), T(\underline{k}) * \left(\hat{p}(-\underline{k})\,\nu(\underline{k})\right)\right) \quad \text{s.t. } \hat{p}(\underline{k}) = \hat{p}_0(\underline{k}) + \sum_{n=1}^{N} c_n \hat{p}_n(k) \quad \forall \underline{k} \in \mathbb{R}^3 \tag{4}$$

yields the non-rigid k-space registration based on optical-flow. The deformation field $\underline{u}$ in the image domain can be directly derived from the all-pass filter

$$\underline{u} = j\frac{\partial\, ln\,\hat{h}(\underline{k})}{\partial \underline{k}}\bigg|_{\underline{k}=\underline{0}} \Leftrightarrow \underline{u} = 2\left[\frac{\sum_{\underline{x}} xp(\underline{x})}{\sum_{\underline{x}} p(\underline{x})}, \frac{\sum_{\underline{x}} yp(\underline{x})}{\sum_{\underline{x}} p(\underline{x})}, \frac{\sum_{\underline{x}} zp(\underline{x})}{\sum_{\underline{x}} p(\underline{x})}\right]^T. \tag{5}$$

### C. Non-rigid registration network

In order to deal with motion of varying strength, a multi-resolution approach is usually applied in which the size of $\mathcal{W}$, respectively the half filter support $\hat{p}$, is decreased, i.e. coarse-to-fine estimation. However, for the k-space based version, summation is required over all $\underline{k}$ positions and for shifted tapering supports. Hence, for carrying out a registration over the complete spectral support requires $2\cdot\left(k_x\cdot k_y\cdot k_z\right)^2$ convolutions at each iteration which can be very demanding. For example for a typical image size of $k_x = k_y = 256, k_z = 144$ would require $178\cdot 10^{12}$ convolutions per multi-resolution level. We seek to simplify these operations by learning an appropriate registration network that can carry out these filter operations. The tapering function $T$ operating on the k-space can be approximated by the computationally more efficient method of cropping in image space and providing the network with patches of k-spaces. As illustrated in Fig. 1, real and imaginary part of the moving and reference k-space are inputted and passed through a succession of 3x3 convolutional filters with dyadic increase in kernel size and leaky ReLU activation function. In the last layer a fully connected regression is performed on the average pooled feature map to estimate the in-plane deformations $\hat{u}_1, \hat{u}_{21}$ at the given central location from the input patch. To obtain a 3D deformation field $\underline{\hat{u}}$, the registration is also performed on an orthogonal direction, yielding $\hat{u}_{22}, \hat{u}_3$ and merged with the previous run to $\hat{u}_x = \hat{u}_1, \hat{u}_y = 0.5(\hat{u}_{21} + \hat{u}_{22}), \hat{u}_z = \hat{u}_3$ . The whole non-rigid deformation field $\underline{\hat{u}}$ is obtained by estimating the deformations $\hat{u}_x, \hat{u}_y, \hat{u}_z$ at all voxel locations. This principle follows the idea of approximating a global non-rigid flow by locally rigid deformations.

The network is trained in a supervised manner on pairs of moving and reference k-space inputs with the corresponding target motion field $\underline{u}$ derived from the LAP [64, 65]. Flows are augmented by smoothing, translating, rotating and shearing. In total 15000 training samples were generated which resulted after tapering in ~150 million training samples. The squared end-point error (sEPE)

$$\text{sEPE} = L_{\text{Reg}} = \sum_i \left(u_{\text{target},i} - \hat{u}_i\right)^2 \tag{6}$$

was employed as the training loss. The network resulted in ~25 million trainable parameters and was trained by an Adam optimizer [72] (learning rate $2.5\cdot 10^{-4}$ with learning rate scheduler, batch size 64) over 150k iterations on a Nvidia V-100 GPU.

### D. Motion-corrected image reconstruction

The network reflects an unrolled ADMM algorithm with cascaded (3+1)D UNets and intermittent data consistency blocks. The network operates on multi-coil complex-valued 4D (3D + time) data. It introduces a series of 3D spatial and 1D temporal complex-valued convolutional filters. The input to the network is the complex-valued subsampled image $\rho$ which was reconstructed with a coil-weighted zero-filling, as well as the acquired k-space $\nu$, the sampling mask $\phi$, the coil sensitivity map $S$ and the motion fields $\underline{\hat{u}}$ from the registration network restacked into the sparse matrix $U \in \mathbb{R}^{N\times N}$.
The unconstrained MR reconstruction problem is given by

$$\arg\min_{\rho} \mathcal{R}(\rho;\Theta) + \lambda\|\phi FSU\rho - \nu\|_2^2 \tag{7}$$

where $F \in \mathbb{C}^{N\times N}$ denotes the discrete Fourier transform, $\|\cdot\|_2$ is the $\ell_2$ norm and $\lambda > 0$ is the data consistency weighting

parameter. The regularizer $\mathcal{R}(\rho;\Theta)$ is expressed by the reconstruction network

$$\mathcal{R}(\rho;\Theta) = \|\rho - f_{\mathrm{Rec}}(\rho_u;\Theta)\|_2^2 \qquad (8)$$

mapping the undersampled image $\rho_u$ to the aliasing-free output image $\rho$ via the feedforward path. The regularizer thus minimizes the complex-valued voxel-wise mean-squared error (MSE). Combining (7) and (8) yields a closed-form solution [73] of the unrolled proximal gradient for the reconstructed k-space

$$v^{k+1} = \begin{cases} Ff_{\mathrm{Rec}}(\rho^k;\Theta), & \phi_n = 0 \\ \frac{1}{1+\lambda}(Ff_{\mathrm{Rec}}(\rho^k;\Theta) + \lambda FU^H S^H F^H \phi v), & \phi_n = 1 \\ \forall n \in [1,N] \end{cases} \quad (9)$$

after stage/iteration $k$ for all voxels and time points which defines consequently the data consistency layer between the sparsity-learning (3+1)D UNet blocks.

The (3+1)D UNet has four encoding and decoding stages which consist of complex-valued spatial convolutional layers of size 3x3x3x1 ($k_x \times k_y \times k_z \times t$) followed by a temporal convolution of size 1x1x1x2 and complex ReLU activation. A complex convolution is performed. A dyadic increase in channel size is selected between stages. Residual paths within stages and between encoder/decoder stages improve convergence. In the encoder branch the last convolutional layer per stage uses a stride of 2 for downsampling between stages while transposed convolutions are performed in the decoder side for upsampling.

For six cascaded (3+1)D UNets, the overall network results in ~5.8 million trainable parameters. It is trained in a supervised manner on retrospectively subsampling the reference data with randomly selected acceleration factors in the range of 3x to 30x. Each training sample is further perturbed with randomly augmented flows (see previous section) yielding in total ~6 million training samples. A complex-valued

$$\mathrm{MSE} = L_{\mathrm{Rec}} = \frac{1}{2}\left\| [\mathrm{Re}(\rho),\ \mathrm{Im}(\rho)]^T - \left[\mathrm{Re}\left(\rho_{\mathrm{target}}\right),\ \mathrm{Im}\left(\rho_{\mathrm{target}}\right)\right]^T \right\|_2^2 \qquad (10)$$

is used as training loss to yield close agreement to the target image $\rho_{\mathrm{target}}$ in a mean-squared error sense. The loss is optimized by Adam [72] (learning rate $10^{-4}$, batch size 16) and fixed data consistency parameter $\lambda = 10^{-3}$ on a Nvidia V-100 GPU for 40 epochs.

### *E. Evaluation and Experiments*

The proposed motion-corrected reconstruction framework was evaluated on prospectively subsampled data in 6 subjects. Motion fields were estimated from subsampled k-space data (~14x accelerated) with the registration network and included into the (3+1)D reconstruction network. For comparison, two image-based 3D registrations using the image-based LAP (denoted as *imageLAP*) [4, 64, 65] and *NiftyReg* [74] were combined with a motion-corrected iterative SENSE reconstruction [27]. Registrations of these methods were performed on initial iterative SENSE reconstructed images. Comparative methods were run on an Intel Xeon E5-2697 CPU.

The end-point error EPE $= \left\|\underline{u} - \underline{u}_{\mathrm{target}}\right\|_2$ and end-angulation error EAE $= \arg(\underline{u}, \underline{u}_{\mathrm{target}})$ between the estimated motion field $\underline{u}$ of the subsampled acquisition was compared with the target motion field $\underline{u}_{\mathrm{target}}$ obtained from an image-based LAP registration of the reference acquisition. Structural similarity index (SSIM) [75] and normalized root MSE (NRMSE) $= 1/N\sqrt{\mathrm{MSE}}$ were calculated between the motion-corrected image $\rho$ and the end-expiratory target $\rho_{\mathrm{target}}$ of the reference scan. All quantitative results are reported as mean ± one standard deviation over all voxel positions and test subjects.

## III. Results

Fig.2 shows the motion-corrected reconstruction in a healthy subject of the proposed framework in comparison to the image-based *imageLAP* and *NiftyReg*. The obtained motion fields are overlaid on the reconstructed and motion-corrected images as a vector field pointing from end-inspiratory ($N_t = 8$) to end-expiratory state. Additionally, the deformation fields are illustrated in coronal and sagittal orientation. It can be appreciated that there exist a significant portion of motion in superior-inferior and anterior-posterior direction. The registration network does not estimate any motion in the image background whereas the image-based methods still try to match background pixels. This helps to minimize background bleeding into image content and reduces noise amplification in the reconstruction. Reconstruction from subsampled images was possible in all cases with a markedly improved visual image quality and sharpness of the proposed approach. For the *imageLAP* and *NiftyReg*, residual blurring of the diaphragm at the lung-liver interface was observed (pointed out by arrows). Visually improved reconstruction quality was obtained with the proposed approach.

In Fig. 3, images of a patient with a metastasis in liver segment V are shown for the proposed approach in comparison to *imageLAP* and *NiftyReg*. The proposed approach provides

Table 1: Quantitative analysis of end-point error (EPE) and end-angulation error (EAE) between estimated deformation field and target deformation field (obtained from image-based LAP in reference scan) in prospectively subsampled acquisition (~14x). Structural similarity index (SSIM) and normalized root mean-squared error (NRMSE) are calculated between the motion-compensated reconstructed image and the end-expiratory target image of the reference scan. Metrics are reported as mean ± one standard deviation for all voxels and test subjects. Best performance is indicated in bold.

| | *Proposed approach* | *imageLAP* | *NiftyReg* |
|---|---|---|---|
| EPE | **0.17 ± 0.26** | 0.97 ± 1.70 | 1.34 ± 1.31 |
| EAE | **7.9° ± 9.9°** | 35.5° ± 22.6° | 40.7° ± 25.3° |
| SSIM | **0.96 ± 0.04** | 0.88 ± 0.07 | 0.81 ± 0.03 |
| NRMSE | **0.005 ± 0.001** | 0.017 ± 0.008 | 0.023 ± 0.01 |

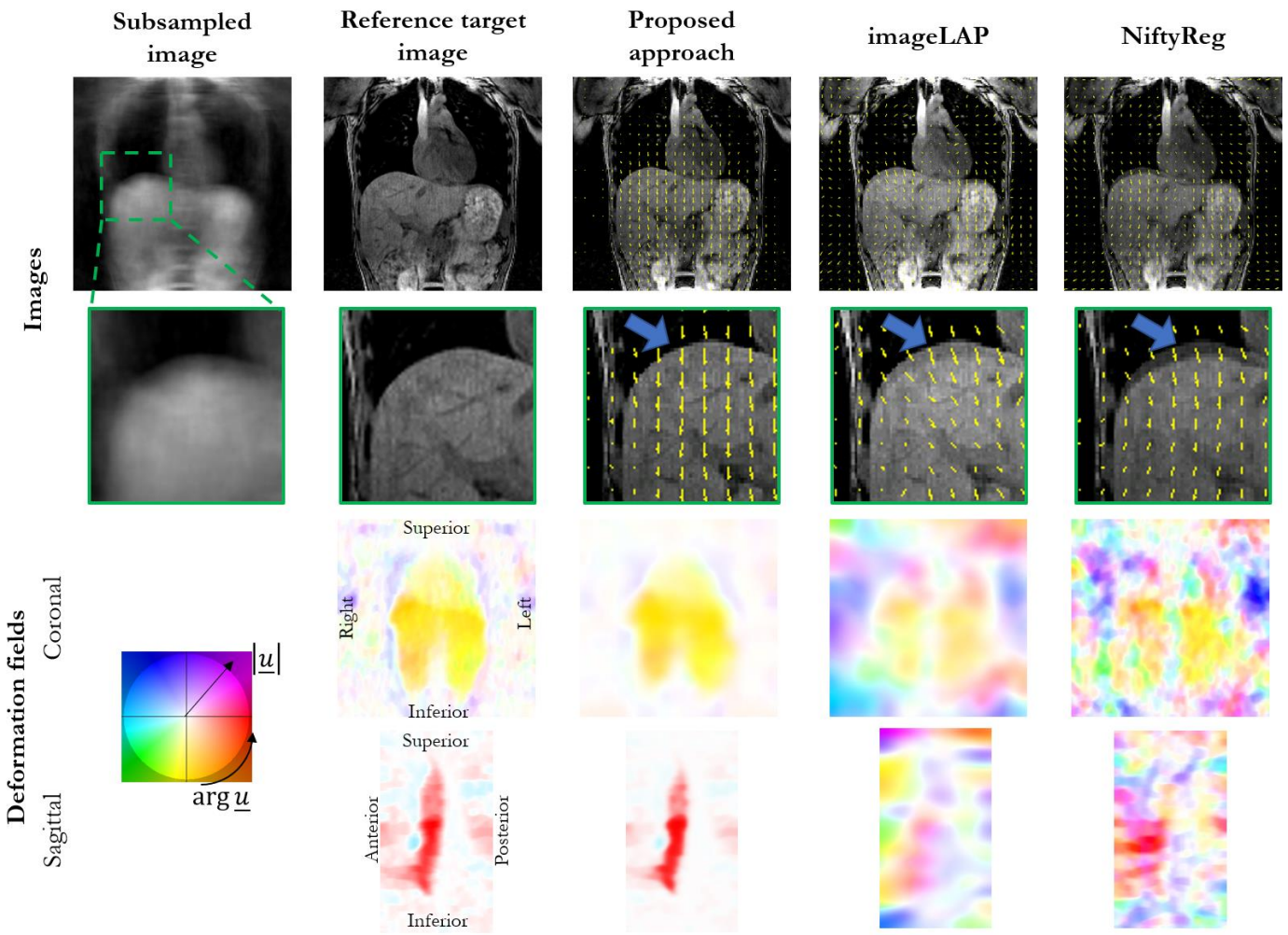


Fig. 2: End-expiratory state of motion-corrected and reconstructed images in a healthy test subject for the proposed approach, image-based LAP registration with motion-corrected iterative SENSE reconstruction and NiftyReg registration with motion-corrected iterative SENSE reconstruction. Zoomed in images of liver dome are depicted. Corresponding deformation fields are shown in coronal and sagittal orientation. A blue arrow points out residual motion blurring at the lung-liver interface.

clear delineation of the liver lesion comparable to the reference scan. Image-based approaches suffer from residual blurring. Good quality images were obtained in an accelerated acquisition of ~90s, reducing scan time and rendering it clinically feasible.

Table 1 summarizes the metrics of the quantitative analysis. The proposed approach outperforms both image-based approaches. It can be seen that any errors in the registration originating from residual aliasing or blurring can propagate into the motion-corrected reconstruction yielding a reduced image quality metric. Consistent and reproducible results were obtained with k-space based registration over the complete cohort.

Training duration of the proposed method was around ~78h. Overall, motion-corrected reconstruction of the proposed method took on average ~35s (registration ~30s, reconstruction ~5s), for *imageLAP* ~841s (registration ~231s, reconstruction ~610s) and for *NiftyReg* ~909s (registration ~301s, reconstruction ~608s), yielding a 25-times faster reconstruction with the proposed approach.

## IV. Discussion

In this work, we proposed the combination of a deep-learning non-rigid k-space registration network with a deep-learning reconstruction network for motion-corrected MR image reconstruction. We investigate the possibility of directly estimating the non-rigid deformation in k-space without the need of a prior image reconstruction. The obtained deformation fields are subsequently incorporated into the motion-corrected reconstruction to enhance spatio-temporal information sharing. An unrolled ADMM algorithm is reflected in a cascade of (3+1)D convolutional layers with intermittent data consistency blocks.

Deformation fields and motion patterns can be different in the reference scan and in the subsampled acquisition. Test subjects were selected which showed good agreement in

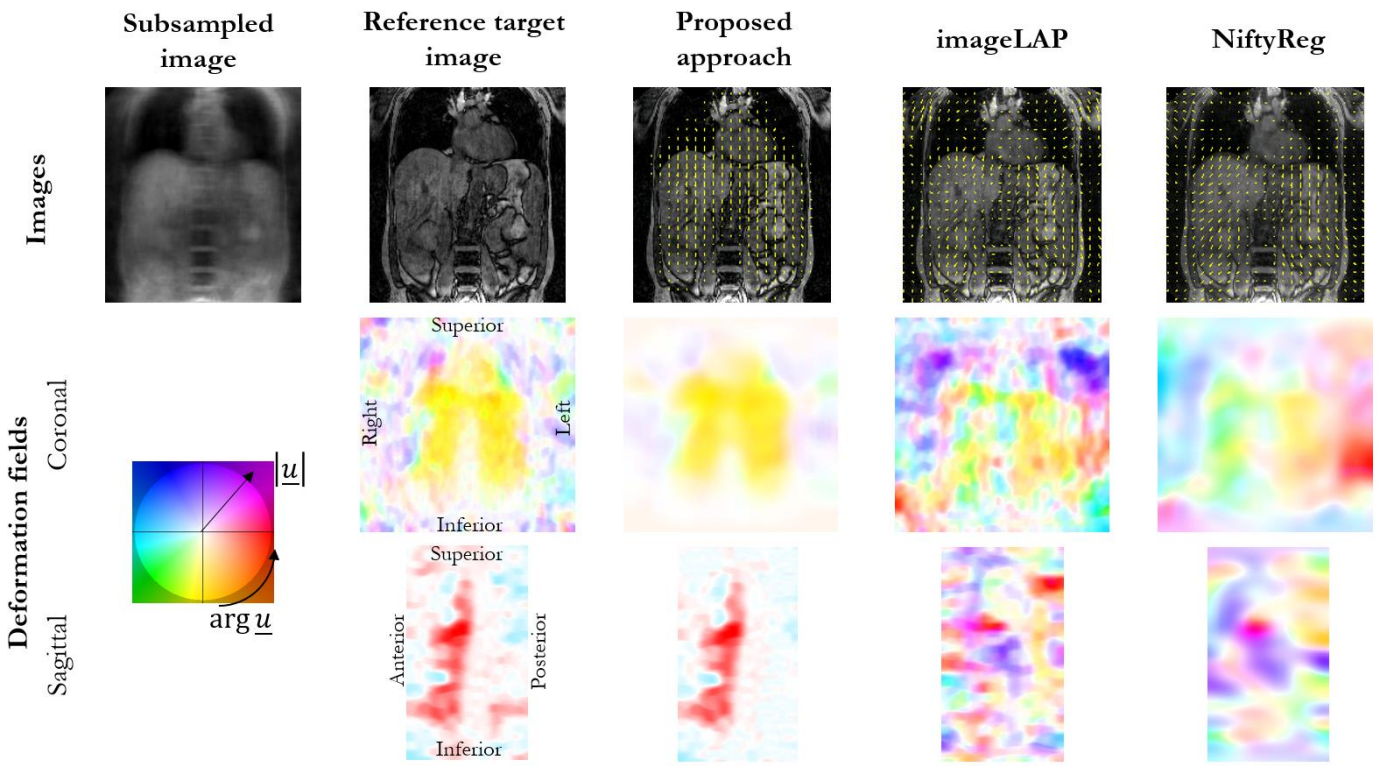


Fig. 3: End-expiratory state of motion-corrected and reconstructed images in a patient with liver metastasis. The proposed approach, image-based LAP registration with motion-corrected iterative SENSE reconstruction and NiftyReg registration with motion-corrected iterative SENSE reconstruction are shown. Corresponding deformation fields are shown in coronal and sagittal orientation.

motion patterns between reference and subsampled acquisition to perform a quantitative analysis with minimal bias. The ground truth target motion field is provided by an image-based LAP registration of the target reference scan. Generation of accurate and reliable ground truth motion fields as well as their evaluation still remain an open challenge [76]. As the registration method for *imageLAP* and for retrieving the target deformation field were the same, one can expect close agreement in quantitative metrics. Hence, any deviation can be mainly attributed to residual aliasing and blurring in the (initially reconstructed) subsampled image. It can thus be a first indicator on how residual aliasing and blurring may influence registration performance when registration is performed in image space. The comparison between *imageLAP* and the registration network (proposed approach) shows thus the impact of performing a registration on accelerated data in image space and in k-space. Please refer to [66], for a comparison of the image-based LAP to the k-space based LAP registration on simulated motion flows.

The non-rigid registration network provided accurate deformation fields which were in close agreement to the target deformation and resembled the true underlying motion. K-space registration showed high agreement with reference motion. For highly accelerated acquisitions, image-based registration can fail whereas k-space registration still provides satisfactory performance. The quantitative analysis of the motion fields yielded good agreement in non-rigid k-space registration with minimal errors.

Continuous and smooth deformations for consecutive motion states were obtained with k-space registration. The registration in k-space was less affected by background noise than the image-based version and deformation fields were concentrated to the actual image content. Static regions (e.g. spine) were not deformed and the largest flow occurred in liver, lung and spleen along head-feet direction. The network-based registration was less computationally demanding than the image-based versions.

The reconstruction network utilized an efficient spatio-temporal redundancy sharing with the proposed (3+1)D convolutional filters. In contrast to a full 4D convolution operation, less trainable parameters were required. Moreover, the estimated deformation fields were incorporated to guide and share samples in the data consistency as well. An unrolled ADMM with a one-step proximal gradient data consistency was formulated for multi-coil complex-valued processing to ensure consistency to acquired raw data. The amount of unrolled reconstruction stages and the regularization parameter were chosen empirically to provide a trade-off between performance and trainable parameters. The networks yield a motion-corrected image and the deformation fields which enable further analysis of the underlying motion.

We acknowledge several limitations of this study. We performed a comparison against established image-based

registration and motion-corrected reconstruction techniques. In the future, other deep learning techniques shall be compared. We did not yet explore the potential of a full end-to-end training, i.e. networks were trained independently with individual loss functions. We anticipate further benefits for jointly training the networks which will be conducted in future studies. A supervised training is performed for the non-rigid registration network which may be impaired by the image-based registration ground-truth. In addition, a full 3D registration may also be beneficial. However, the obtained results in this study did not indicate any significant performance loss of the supervised pseudo 3D training scheme. Replacing the one-step proximal gradient data consistency by a conjugate gradient might enhance convergence speed. The proposed approach was only tested for respiratory motion in T1-weighted imaging of the body trunk. Future studies will investigate its generalizability to different imaging applications and sequences. A Cartesian subsampling was performed which results in incoherent aliasing artifacts along phase-encoding directions. For radial or spiral subsampling, different aliasing artifacts will manifest in the image and may require a retraining.

## V. Conclusion

A deep-learning based motion-corrected reconstruction network was proposed which combines a non-rigid k-space registration network with a (3+1)D reconstruction network. Non-rigid registration in k-space is feasible and provides reliable deformation fields especially for highly accelerated imaging for which image-based registration is impaired. Incorporating the deformation fields into the reconstruction network allows for efficient utilization of spatio-temporal information. The proposed approach was in close agreement with the ground-truth and provided 4D motion-corrected images and deformation fields within ~35s.

## Acknowledgment

The authors would like to thank Brigitte Gückel for study coordination as well as Carsten Groeper and Gerd Zeger for data acquisition.

## References

[1] J. R. McClelland, J. M. Blackall, S. Tarte, A. C. Chandler, S. Hughes, S. Ahmad, D. B. Landau, and D. J. Hawkes, "A continuous 4D motion model from multiple respiratory cycles for use in lung radiotherapy," *Medical Physics,* vol. 33, no. 9, pp. 3348-3358, 2006.

[2] D. Manke, K. Nehrke, P. Börnert, P. Rösch, and O. Dössel, "Respiratory motion in coronary magnetic resonance angiography: a comparison of different motion models," *Journal of Magnetic Resonance Imaging,* vol. 15, no. 6, pp. 661-671, 2002.

[3] C. Munoz, R. Neji, G. Cruz, A. Mallia, S. Jeljeli, A. J. Reader, R. M. Botnar, and C. Prieto, "Motion-corrected simultaneous cardiac positron emission tomography and coronary MR angiography with high acquisition efficiency," *Magnetic Resonance in Medicine,* vol. 79, no. 1, pp. 339-350, 2018.

[4] T. Küstner, M. Schwartz, P. Martirosian, S. Gatidis, F. Seith, C. Gilliam, T. Blu, H. Fayad, D. Visvikis, and F. Schick, "MR-based respiratory and cardiac motion correction for PET imaging," *Medical image analysis,* vol. 42, pp. 129-144, 2017.

[5] M. A. Griswold, P. M. Jakob, R. M. Heidemann, M. Nittka, V. Jellus, J. Wang, B. Kiefer, and A. Haase, "Generalized autocalibrating partially parallel acquisitions (GRAPPA)," *Magnetic Resonance in Medicine,* vol. 47, no. 6, pp. 1202-1210, 2002.

[6] M. Lustig, D. Donoho, and J. M. Pauly, "Sparse MRI: The application of compressed sensing for rapid MR imaging," *Magnetic Resonance in Medicine,* vol. 58, no. 6, pp. 1182-1195, 2007.

[7] M. Henningsson, P. Koken, C. Stehning, R. Razavi, C. Prieto, and R. M. Botnar, "Whole-heart coronary MR angiography with 2D self-navigated image reconstruction," *Magnetic Resonance in Medicine,* vol. 67, no. 2, pp. 437-445, 2012.

[8] S. Skare, A. Hartwig, M. Martensson, E. Avventi, and M. Engstrom, "Properties of a 2D fat navigator for prospective image domain correction of nodding motion in brain MRI," *Magnetic Resonance in Medicine,* vol. 73, no. 3, pp. 1110-9, Mar, 2015.

[9] J. Y. Cheng, M. T. Alley, C. H. Cunningham, S. S. Vasanawala, J. M. Pauly, and M. Lustig, "Nonrigid motion correction in 3D using autofocusing with localized linear translations," *Magnetic Resonance in Medicine,* vol. 68, no. 6, pp. 1785-97, Dec, 2012.

[10] T. Kober, J. P. Marques, R. Gruetter, and G. Krueger, "Head motion detection using FID navigators," *Magnetic Resonance in Medicine,* vol. 66, no. 1, pp. 135-143, 2011.

[11] T. E. Wallace, O. Afacan, M. Waszak, T. Kober, and S. K. Warfield, "Head motion measurement and correction using FID navigators," *Magnetic Resonance in Medicine,* vol. 81, no. 1, pp. 258-274, 2019.

[12] N. White, C. Roddey, A. Shankaranarayanan, E. Han, D. Rettmann, J. Santos, J. Kuperman, and A. Dale, "PROMO: real-time prospective motion correction in MRI using image-based tracking," *Magnetic Resonance in Medicine,* vol. 63, no. 1, pp. 91-105, 2010.

[13] J. Maclaren, M. Herbst, O. Speck, and M. Zaitsev, "Prospective motion correction in brain imaging: a review," *Magnetic Resonance in Medicine,* vol. 69, no. 3, pp. 621-636, 2013.

[14] M. Zaitsev, J. Maclaren, and M. Herbst, "Motion artifacts in MRI: A complex problem with many partial solutions," *Journal of Magnetic Resonance Imaging,* vol. 42, no. 4, pp. 887-901, Oct, 2015.

[15] K. T. Block, M. Uecker, and J. Frahm, "Undersampled radial MRI with multiple coils. Iterative image reconstruction using a total variation constraint," *Magnetic Resonance in Medicine,* vol. 57, no. 6, pp. 1086-1098, 2007.

[16] O. Speck, J. Hennig, and M. Zaitsev, "Prospective real-time slice-by-slice motion correction for fMRI in freely moving subjects," *Magnetic Resonance Materials in Physics, Biology and Medicine,* vol. 19, no. 2, pp. 55, 2006.

[17] J. Y. Cheng, T. Zhang, N. Ruangwattanapaisarn, M. T. Alley, M. Uecker, J. M. Pauly, M. Lustig, and S. S. Vasanawala, "Free-breathing pediatric MRI with nonrigid

motion correction and acceleration," *Journal of Magnetic Resonance Imaging,* vol. 42, no. 2, pp. 407-420, 2015.

[18] F. Han, Z. Zhou, E. Han, Y. Gao, K. L. Nguyen, J. P. Finn, and P. Hu, "Self-gated 4D multiphase, steady-state imaging with contrast enhancement (MUSIC) using rotating cartesian K-space (ROCK): Validation in children with congenital heart disease," *Magnetic Resonance in Medicine,* vol. 78, no. 2, pp. 472-483, 2017.

[19] G. Cruz, D. Atkinson, M. Henningsson, R. M. Botnar, and C. Prieto, "Highly efficient nonrigid motion-corrected 3D whole-heart coronary vessel wall imaging," *Magnetic Resonance in Medicine,* vol. 77, no. 5, pp. 1894-1908, 2017.

[20] T. Küstner, C. Würslin, M. Schwartz, P. Martirosian, S. Gatidis, C. Brendle, F. Seith, F. Schick, N. F. Schwenzer, and B. Yang, "Self-navigated 4D cartesian imaging of periodic motion in the body trunk using partial k-space compressed sensing," *Magnetic Resonance in Medicine,* vol. 78, no. 2, pp. 632-644, 2017.

[21] R. Otazo, E. Candes, and D. K. Sodickson, "Low-rank plus sparse matrix decomposition for accelerated dynamic MRI with separation of background and dynamic components," *Magnetic resonance in medicine,* vol. 73, no. 3, pp. 1125-1136, 2015.

[22] J.-P. Thirion, "Image matching as a diffusion process: an analogy with Maxwell's demons," *Medical image analysis,* vol. 2, no. 3, pp. 243-260, 1998.

[23] D. Rueckert, L. I. Sonoda, C. Hayes, D. L. Hill, M. O. Leach, and D. J. Hawkes, "Nonrigid registration using free-form deformations: application to breast MR images," *IEEE Transactions on Medical Imaging,* vol. 18, no. 8, pp. 712-721, 1999.

[24] B. K. Horn, and B. G. Schunck, "Determining optical flow," *Artificial intelligence,* vol. 17, no. 1-3, pp. 185-203, 1981.

[25] F. Odille, P. A. Vuissoz, P. Y. Marie, and J. Felblinger, "Generalized reconstruction by inversion of coupled systems (GRICS) applied to free-breathing MRI," *Magnetic Resonance in Medicine,* vol. 60, no. 1, pp. 146-157, 2008.

[26] L. Cordero-Grande, R. P. A. Teixeira, E. J. Hughes, J. Hutter, A. N. Price, and J. V. Hajnal, "Sensitivity encoding for aligned multishot magnetic resonance reconstruction," *IEEE Transactions on Computational Imaging,* vol. 2, no. 3, pp. 266-280, 2016.

[27] P. Batchelor, D. Atkinson, P. Irarrazaval, D. Hill, J. Hajnal, and D. Larkman, "Matrix description of general motion correction applied to multishot images," *Magnetic Resonance in Medicine,* vol. 54, no. 5, pp. 1273-1280, 2005.

[28] D. Atkinson, D. L. Hill, P. N. Stoyle, P. E. Summers, and S. F. Keevil, "Automatic correction of motion artifacts in magnetic resonance images using an entropy focus criterion," *IEEE Transactions on Medical Imaging,* vol. 16, no. 6, pp. 903-10, Dec, 1997.

[29] F. Ong, and M. Lustig, "Joint Non-Rigid Motion Estimation and Image Reconstruction via Sparse Blind Deconvolution." p. 3937.

[30] M. W. Haskell, S. F. Cauley, B. Bilgic, J. Hossbach, D. N. Splitthoff, J. Pfeuffer, K. Setsompop, and L. L. Wald, "Network Accelerated Motion Estimation and Reduction (NAMER): Convolutional neural network guided retrospective motion correction using a separable motion model," *Magnetic Resonance in Medicine,* vol. 82, no. 4, pp. 1452-1461, 2019.

[31] M. Usman, S. Latif, M. Asim, and J. Qadir, "Motion Corrected Multishot MRI Reconstruction Using Generative Networks with Sensitivity Encoding," *arXiv preprint arXiv:1902.07430,* 2019.

[32] F. Liu, D. Li, X. Jin, W. Qiu, Q. Xia, and B. Sun, "Dynamic cardiac MRI reconstruction using motion aligned locally low rank tensor (MALLRT)," *Magnetic Resonance Imaging,* vol. [Epub ahead of print], 2019/07/03/, 2019.

[33] Y. Q. Mohsin, S. G. Lingala, E. DiBella, and M. Jacob, "Accelerated dynamic MRI using patch regularization for implicit motion compensation," *Magnetic Resonance in Medicine,* vol. 77, no. 3, pp. 1238-1248, Mar, 2017.

[34] S. G. Lingala, Y. Hu, E. DiBella, and M. Jacob, "Accelerated dynamic MRI exploiting sparsity and low-rank structure: kt SLR," *IEEE Transactions on Medical Imaging,* vol. 30, no. 5, pp. 1042-1054, 2011.

[35] X. Chen, M. Salerno, Y. Yang, and F. H. Epstein, "Motion-compensated compressed sensing for dynamic contrast-enhanced MRI using regional spatiotemporal sparsity and region tracking: Block low-rank sparsity with motion-guidance (BLOSM)," *Magnetic Resonance in Medicine,* vol. 72, no. 4, pp. 1028-1038, 2014.

[36] J. Caballero, A. N. Price, D. Rueckert, and J. V. Hajnal, "Dictionary Learning and Time Sparsity for Dynamic MR Data Reconstruction," *IEEE Trans Med Imag,* vol. 33, no. 4, pp. 979-994, 2014.

[37] H. Jung, J. C. Ye, and E. Y. Kim, "Improved k-t BLAST and k-t SENSE using FOCUSS," *Phys Med Biol,* vol. 52, no. 11, pp. 3201-26, Jun 7, 2007.

[38] T. Küstner, A. Bustin, O. Jaubert, R. Hajhosseiny, P. G. Masci, R. Neji, R. Botnar, and C. Prieto, "Isotropic 3D Cartesian single breath-hold CINE MRI with multi-bin patch-based low-rank reconstruction," *Magnetic Resonance in Medicine,* 2020.

[39] A. S. Lundervold, and A. Lundervold, "An overview of deep learning in medical imaging focusing on MRI," *Z Med Phys,* vol. 29, no. 2, pp. 102-127, 2019/05/01/, 2019.

[40] F. Knoll, K. Hammernik, C. Zhang, S. Moeller, T. Pock, D. K. Sodickson, and M. Akcakaya, "Deep learning methods for parallel magnetic resonance image reconstruction," *arXiv preprint arXiv:1904.01112,* 2019.

[41] C. M. Hyun, H. P. Kim, S. M. Lee, S. Lee, and J. K. Seo, "Deep learning for undersampled MRI reconstruction," *Phys Med Biol,* vol. 63, no. 13, pp. 135007, 2018.

[42] D. J. Lin, P. M. Johnson, F. Knoll, and Y. W. Lui, "Artificial Intelligence for MR Image Reconstruction: An Overview for Clinicians," *J Magn Reson Imag,* 2020.

[43] J. Sun, H. Li, and Z. Xu, "Deep ADMM-Net for compressive sensing MRI." pp. 10-18.

[44] T. Eo, Y. Jun, T. Kim, J. Jang, H.-J. Lee, and D. Hwang, "KIKI-net: cross-domain convolutional neural networks for reconstructing undersampled magnetic resonance images," *Magn Reson Med,* vol. 80, no. 5, pp. 2188-2201, 2018.

[45] J. Schlemper, J. Caballero, J. V. Hajnal, A. N. Price, and D. Rueckert, "A deep cascade of convolutional neural networks for dynamic MR image reconstruction," *IEEE Trans Med Imag,* vol. 37, no. 2, pp. 491-503, 2017.

[46] S. Wang, Z. Su, L. Ying, X. Peng, S. Zhu, F. Liang, D. Feng, and D. Liang, "Accelerating magnetic resonance imaging via deep learning." pp. 514-517.

[47] Y. Han, L. Sunwoo, and J. C. Ye, "k-space deep learning for accelerated MRI," *IEEE Trans Med Imag,* vol. 39, no. 2, pp. 377-386, 2019.

[48] C. Qin, J. Schlemper, J. Caballero, A. N. Price, J. V. Hajnal, and D. Rueckert, "Convolutional Recurrent Neural

Networks for Dynamic MR Image Reconstruction," *IEEE Trans Med Imag*, vol. 38, no. 1, pp. 280-290, 2019.

[49] G. Yang, S. Yu, H. Dong, G. Slabaugh, P. L. Dragotti, X. Ye, F. Liu, S. Arridge, J. Keegan, Y. Guo, and D. Firmin, "DAGAN: Deep De-Aliasing Generative Adversarial Networks for Fast Compressed Sensing MRI Reconstruction," *IEEE Trans Med Imag*, vol. 37, no. 6, pp. 1310-1321, 2018.

[50] M. Mardani, E. Gong, J. Y. Cheng, S. S. Vasanawala, G. Zaharchuk, L. Xing, and J. M. Pauly, "Deep generative adversarial neural networks for compressive sensing MRI," *IEEE Trans Med Imag*, vol. 38, no. 1, pp. 167-179, 2018.

[51] B. Zhu, J. Z. Liu, S. F. Cauley, B. R. Rosen, and M. S. Rosen, "Image reconstruction by domain-transform manifold learning," *Nature*, vol. 555, no. 7697, pp. 487-492, 2018.

[52] K. Hammernik, T. Klatzer, E. Kobler, M. P. Recht, D. K. Sodickson, T. Pock, and F. Knoll, "Learning a variational network for reconstruction of accelerated MRI data," *Magn Reson Med*, vol. 79, no. 6, pp. 3055-3071, 2018.

[53] F. Chen, V. Taviani, I. Malkiel, J. Y. Cheng, J. I. Tamir, J. Shaikh, S. T. Chang, C. J. Hardy, J. M. Pauly, and S. S. Vasanawala, "Variable-density single-shot fast spin-echo MRI with deep learning reconstruction by using variational networks," *Radiology*, vol. 289, no. 2, pp. 366-373, 2018.

[54] N. Fuin, A. Bustin, T. Küstner, R. Botnar, and C. Prieto, "A Variational Neural Network for Accelerating Free-breathing Whole-Heart Coronary MR Angiography." p. 478.

[55] J. Y. Cheng, M. Mardani, M. T. Alley, J. M. Pauly, and S. S. Vasanawala, "DeepSPIRiT: Generalized Parallel Imaging using Deep Convolutional Neural Networks." p. 570.

[56] C. M. Sandino, P. Lai, S. S. Vasanawala, and J. Y. Cheng, "DL-ESPIRiT: Improving robustness to SENSE model errors in deep learning-based reconstruction." p. 659.

[57] S. A. H. Hosseini, C. Zhang, S. Weingärtner, S. Moeller, M. Stuber, K. Ugurbil, and M. Akçakaya, "Accelerated coronary MRI with sRAKI: A database-free self-consistent neural network k-space reconstruction for arbitrary undersampling," *PLOS ONE*, vol. 15, no. 2, 2020.

[58] D. Lee, J. Yoo, S. Tak, and J. C. Ye, "Deep Residual Learning for Accelerated MRI Using Magnitude and Phase Networks," *IEEE Trans Biomed Eng*, vol. 65, no. 9, pp. 1985-1995, 2018.

[59] C. M. Sandino, P. Lai, S. S. Vasanawala, and J. Y. Cheng, "Accelerating cardiac cine MRI beyond compressed sensing using DL-ESPIRiT," *arXiv preprint arXiv:1911.05845*, 2019.

[60] F. Chen, J. Y. Cheng, V. Taviani, V. R. Sheth, R. L. Brunsing, J. M. Pauly, and S. S. Vasanawala, "Data-driven self-calibration and reconstruction for non-cartesian wave-encoded single-shot fast spin echo using deep learning," *J Magn Reson Imag*, vol. 51, no. 3, pp. 841-853, 2020.

[61] M. O. Malavé, C. A. Baron, S. P. Koundinyan, C. M. Sandino, F. Ong, J. Y. Cheng, and D. G. Nishimura, "Reconstruction of Undersampled 3D Non-Cartesian Image-Based Navigators for Coronary MRA Using an Unrolled Deep Learning Model," *arXiv preprint arXiv:1910.11414*, 2019.

[62] Q. Huang, D. Yang, H. Qu, J. Yi, P. Wu, and D. Metaxas, "Dynamic MRI Reconstruction with Motion-Guided Network," in Proceedings of The 2nd International Conference on Medical Imaging with Deep Learning, Proceedings of Machine Learning Research, 2019, pp. 275--284.

[63] G. Seegoolam, J. Schlemper, C. Qin, A. Price, J. V. Hajnal, and D. Rueckert, "Exploiting Motion for Deep Learning Reconstruction of Extremely-Undersampled Dynamic MRI."

[64] C. Gilliam, T. Küstner, and T. Blu, "3D motion flow estimation using local all-pass filters." pp. 282-285.

[65] T. Küstner, M. Schwartz, S. Gatidis, N. F. Schwenzer, H. Schmidt, B. Yang, C. Gilliam, T. Blu, and F. Schick, "Local All-Pass Filter (LAP): Efficient Optical Flow-Based Image Registration."

[66] T. Küstner, C. Gilliam, T. Blu, M. Schwartz, G. Cruz, J. Pan, C. Würslin, N. F. Schwenzer, H. Schmidt, and B. Yang, "Non-rigid "image" registration in k-space."

[67] T. Küstner, C. Würslin, S. Gatidis, P. Martirosian, K. Nikolaou, N. Schwenzer, F. Schick, B. Yang, and H. Schmidt, "MR Image Reconstruction Using a Combination of Compressed Sensing and Partial Fourier Acquisition: ESPReSSo," *IEEE Transactions on Medical Imaging*, vol. 35, no. 11, pp. 2447-2458, 2016.

[68] M. Uecker, P. Lai, M. J. Murphy, P. Virtue, M. Elad, J. M. Pauly, S. S. Vasanawala, and M. Lustig, "ESPIRiT—an eigenvalue approach to autocalibrating parallel MRI: Where SENSE meets GRAPPA," *Magn Reson Med*, vol. 71, no. 3, pp. 990-1001, 2014.

[69] K. P. Pruessmann, M. Weiger, P. Börnert, and P. Boesiger, "Advances in sensitivity encoding with arbitrary k-space trajectories," *Magnetic Resonance in Medicine*, vol. 46, no. 4, pp. 638-651, 2001.

[70] C. Gilliam, and T. Blu, "Local all-pass filters for optical flow estimation." pp. 1533-1537.

[71] T. Blu, P. Moulin, and C. Gilliam, "Approximationorder of the lap optical flow algorithm." pp. 48-52.

[72] D. P. Kingma, and J. Ba, "Adam: A method for stochastic optimization," *arXiv preprint arXiv:1412.6980*, 2014.

[73] S. Ravishankar, and Y. Bresler, "MR Image Reconstruction From Highly Undersampled k-Space Data by Dictionary Learning," *IEEE Transactions on Medical Imaging*, vol. 30, no. 5, pp. 1028-1041, 2011.

[74] M. Modat, G. R. Ridgway, Z. A. Taylor, M. Lehmann, J. Barnes, D. J. Hawkes, N. C. Fox, and S. Ourselin, "Fast free-form deformation using graphics processing units," *Computer Methods and Programs in Biomedicine*, vol. 98, no. 3, pp. 278-284, 2010/06/01/, 2010.

[75] W. Zhou, A. C. Bovik, H. R. Sheikh, and E. P. Simoncelli, "Image quality assessment: from error visibility to structural similarity," *IEEE Transactions on Image Processing*, vol. 13, no. 4, pp. 600-612, 2004.

[76] T. Rohlfing, C. Maurer, W. O'Dell, and J. Zhong, "Modeling liver motion and deformation during the respiratory cycle using intensity-based free-form registration of gated MR images," *Medical Imaging*, vol. 4319, 2001.